Journal of Polymer Research (2023) 30:103
https://doi.org/10.1007/s10965-023-03461-8

ORIGINAL PAPER

ZnO-containing nanocomposites produced from *Mentha pulegium* L. of a new HEMA-based methacrylate copolymer: improvement the thermal and antimicrobial effect

Ibrahim Erol[1,3] · Merve Sivrier[1] · Ibrahim Hakkı Cigerci[2] · Arzu Özkara[2] · Dilek Akyıl[2]

Received: 26 August 2022 / Accepted: 9 January 2023 / Published online: 11 February 2023

Abstract
In this study, firstly, (2-oxo-2-(3,4,5-trifluoroanilino)-ethyl-2-methylprop-2-enoate) FAOEME, a methacrylate monomer with arylamide side group containing three fluorine atoms in the side branch, was synthesized. Poly(HEMA-co-FAOEME) was obtained due to radical copolymerization of FAOEME with 2-hydroxyethyl methacrylate (HEMA). Structural characterization of its copolymer with FAOEME and HEMA was performed by spectroscopy methods such as FTIR, ^{1}H, and ^{13}C-NMR. Biosynthesis of ZnO nanoparticles was carried out using *Mentha Plegium* L. extract. Three nanocomposites of poly(HEMA-co-FAOEME) containing biosynthesized ZnO nanoparticles were produced by hydrothermal technique, which is an environmentally friendly method. The formation of Poly(HEMA-co-FAOEME)/ZnO nanocomposites and the structural changes of the components was elucidated by SEM, XRD, and FTIR techniques. The effect of ZnO nanoparticles on the thermal properties of Poly(HEMA-co-FAOEME) was investigated by TGA and DSC techniques. The results showed that ZnO nanoparticles significantly increased the thermal stability and glass transition temperature (Tg) of the matrix (poly(HEMA-co-FAOEME). The antimicrobial properties of the materials were determined by the disk diffusion method using five different bacteria and one yeast cell. It was observed that the nanocomposites showed activity against all pathogens except one bacterial species, and the source of the activity was ZnO nanoparticles.

Keywords HEMA · *Mentha pulegium* L. · ZnO nanoparticle · Hydrothermal method · Antimicrobial activity

Introduction

The pandemic process we are currently experiencing has clearly shown that more effective protection methods against viruses and bacteria should be developed. In addition to effective protection tools such as vaccines and drugs against pathogens, it has become essential to provide antibacterial and antiviral properties to many materials we use in our daily lives and to reduce infection rates [1–3]. By using appropriate chemical methods, biological agents can be added to plastics, food packaging, and biomedical materials that we frequently use in our daily lives to gain biological properties [4, 5]. Material hybridization has been a frequently used approach to produce polymer materials with improved properties and functionality. In recent years, nanomaterials have attracted attention with their prominent biological activities and their use in different medical applications. Different metal oxide nanoparticles are seen as promising materials with wide use in medical and biomedical fields [6, 7].

Poly(2-hydroxyethyl methacrylate) (PHEMA) is a biocompatible polymer used in biomedical applications [8–10]. Recent studies have shown that HEMA-based nanocomposites are highly effective against *S. aures* and *E. coli* bacteria [11, 12].

It has been reported that some polymers containing fluorine atoms in the side branch are widely used especially in construction, automotive, aerospace, optics and microelectronic technologies due to their superior properties [13, 14]. In recent studies, it has been observed that methacrylate-based fluorine-containing copolymers and nanocomposites

✉ Ibrahim Erol
ierol@aku.edu.tr

[1] Faculty of Science and Arts, Department of Chemistry, Afyon Kocatepe University, Afyonkarahisar 03200, Turkey

[2] Faculty of Science and Arts, Department of Molecular Biology and Genetic, Afyon Kocatepe University, Afyonkarahisar 03200, Turkey

[3] Faculty of Chemistry, Department of Polymer Chemistry and Chemical Technology, Samarkand State University, University bvld-15, Samarkand, Uzbekistan

are quite effective against some pathogens [15, 16]. Due to their low economic cost and toxicity, ZnO nanoparticles (NPs) are used as preservatives and packaging in the food industry [17]. It has been stated in various studies [18, 19] that ZnO NPs can show antibacterial activity even at low concentrations. Due to these properties, ZnO NPs are widely used as drug carriers [20], cosmetic products, nutritional preservatives [21], plasters, and filling medical materials. In addition to these features, the fact that ZnO NPs have antiviral activity [22] suggests that they can be used to develop valuable products against SARS-CoV 2 virus.

Mentha pulegium L., a member of the Labiatae family, grows in Africa, Temperate Asia and Europe [23]. It is a perennial herb with an underground root system and a 10–40 cm high stem with a pungent odor that spreads rapidly throughout the ground. *Mentha pulegium L.* essential oils, which are colorless, pale yellow or pale greenish yellow, liquid and have a characteristic odor, contain menthol, menthyl acetate, carvone and pulegon/piperitone [24]. The flavonoid compounds contained in *Mentha pulegium* L. species are hesperidin, apigenin, luteolin and rutin [25]. It has been reported in the literature that *Mentha pulegium* L. has anti-inflammatory and anti-oxidative [26], antigenotoxic [27] and antibacterial [28, 29] effects.

As can be seen from the literature studies, it is important to produce different materials such as copolymer and composite that will improve the biological and thermal properties of HEMA commercial polymer. Such properties can be imparted by incorporating functional structures into commercial polymers through chemical modification. It can be expected that the strong interactions between fluorine atoms and the hydroxyl groups in the HEMA structure will create synergistic effects with ZnO NPs, giving the copolymer structure the expected superior properties. In addition, choosing the hydrothermal method, which is an environmentally friendly application, is an example of a good green synthesis application in the production of nanocomposites.

In this study, 2-oxo-2-(3,4,5-trifluoroanilino)ethyl-2-methylprop-2-enoate (FAOEME), a new methacrylate monomer containing fluoroarylamide in the side branch, was synthesized and then copolymerized with a commercial monomer, HEMA. Then, three different nanocomposites of the obtained copolymer were produced by hydrothermal method using ZnO nanoparticles obtained from *Mentha pulegium* L. The effect of biosynthetic ZnO nanoparticles on the antimicrobial and thermal properties of the obtained nanocomposites was investigated in detail. The results showed that the newly synthesized nanocomposites have high resistance to gram-negative, gram-positive, and yeast microorganisms and can show biomaterial properties. It has been reported in the literature that polymeric nanomaterials with superior properties can be obtained by the hydrothermal method [30, 31].

Materials and methods

Materials

2-Hydroxyethyl methacrylate (HEMA), 3,4,5-trifluoroaniline, chloroacetyl chloride and sodium methacrylate were obtained from Merck (Germany) and used without any purification. Azobisisobutyronitrile (AIBN) (Aldrich, Germany) was recrystallized from a chloroform-methanol mixture. HEMA was used purified according to the reliable method described in the literature [32]. Since the solvents used in the studies were of high purity (≥98%), they were used as supplied without any purification.

Synthesis of 2-oxo-2-(3,4,5-trifluoroanilino) ethyl-2-methylprop-2-enoate (FAOEME)

FAOEME monomer was synthesized in two steps as indicated in the literature [33]. First, the intermediate 2-Chloro-N-(3,4,5-trifluorophenyl)acetamide (I) was obtained as follows; 10 g (68 mmol) of 3,4,5-trifluoroaniline, 9 g potassium carbonate and 30 mL dichloromethane were placed in a reaction flask and 5.90 mL (75 mmol) chloroacetyl chloride was added dropwise at 0 °C, and the reaction was continued for 12 h. When the time was up, the product was filtered and crystallized from ethanol. Product yield was recorded as 75%. For the synthesis of FAOEME monomer, 11.8 g (53 mmol) of 2-Chloro-N-(3,4,5-trifluorophenyl)acetamide was reacted with 6.34 g (58 mmol) sodium methacrylate in acetonitrile solvent (60 mL) in a reaction flask at 80 °C for 24 h. After the reaction was complete, the product was extracted three times with diethyl ether, dried over MgSO4, and crystallized from n-hexane. The reaction yield was 80%. Monomer synthesis steps are shown in Scheme 1.

Synthesis of poly(HEMA-co-FAOEME)

Poly(HEMA-co-FAOEME) was prepared according to the following procedure; 1 g of FAOEME, 0.44 mL of HEMA, AIBN (0.028 g) as initiator and 4 mL 1,4-dioxane solvent were placed in a polymers tube. Nitrogen gas was then passed through the mixture for 10 min and copolymerized in an oil bath at 65 °C for 24 h. The resulting copolymer was filtered by precipitation in ethanol and dried in a vacuum oven at 70 °C for 4 h. Copolymer synthesis is shown in Scheme 2.

Biosynthesis of ZnO nanoparticles from *Mentha pulegium L.*

Biosynthesis of zinc nanoparticles was carried out with the aerial parts of *Mentha pulegium L.* taken commercially. 5 g of *Mentha pulegium* L. in powder form was mixed with 100 mL

Scheme 1 FAOEME synthesis steps

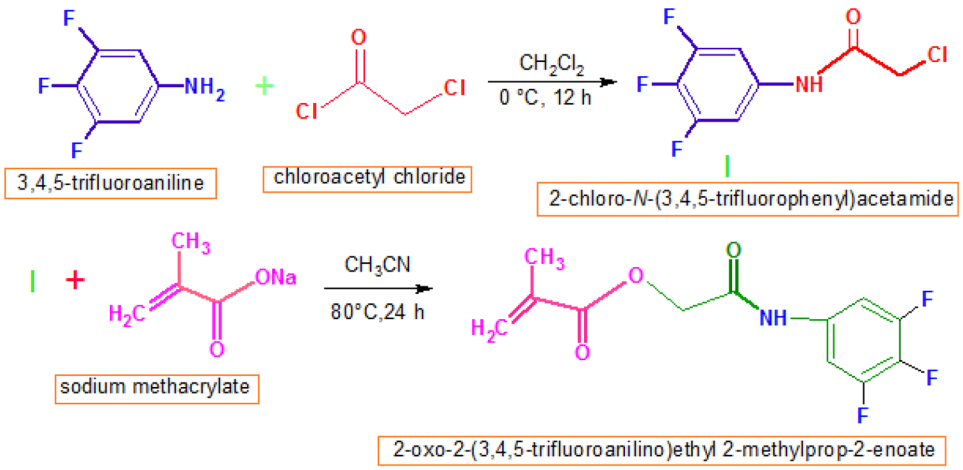

of dH_2O in a beaker and boiled on a heat shaker at 60 °C for 15 min. Then it was filtered into a glass bottle with Whatman no:1 paper. 20 mL of the extract from the filtrate was placed in a beaker, and 100 mL of 0.1 M zinc acetate solution was added to it and mixed with a mechanical mixer at room temperature for one hour. At the end of the period, the mixture was centrifuged at 3000 rpm for 10 min. The resulting ZnO nanoparticles were dried in an oven at 60 °C for 4 h.

Preparation of poly(HEMA-co-FAOEME)/ZnO nanocomposites

Nanocomposites containing poly(HEMA-co-FAOEME) as a matrix and biosynthetic ZnO nanoparticles in different weight ratios (3%, 5%, 7%) were produced by the hydrothermal method. Detailed information on the preparation of nanocomposites is presented in Table 1.

A typical method used to obtain nanocomposites is as follows; The copolymer matrix and ZnO nanoparticles, the amounts of which were determined, were placed in a Teflon container, and 30 mL of water was added to them. Then, to ensure the mixture's homogeneous distribution, the first half an hour with a mechanical mixer and then 20 min with an ultrasonic probe were mixed. The homogenized mixture was placed in the hydrothermal synthesis device and incubated at 150 °C for 24 h. The resulting nanocomposites were filtered, washed with water, and dried in a vacuum oven at 70 °C for 6 h.

Antimicrobial properties of ZnO nanoparticles and nanocomposites

The antibacterial activity analysis of the ZnO and nanocomposites was performed using Kirby-Bauer Disk Diffusion Susceptibility Test [34] against different microorganisms and yeasts. In this study, a yeast *Candida krusei* (ATCC 6258) and five different bacterial strains; *Escherichia coli* culture (ATCC) 25922), *Staphylaccocus aureus* (ATCC 29213) and *Pseudomonas aeruginosa*, *Enterecoccus faecalis* (ATCC 29212), *Klebsiella pneumoniae* were studied and microorganisms were obtained from Akdeniz University and Afyon Health Sciences University, Department of Microbiology. Disk diffusion method was carried out in Afyon Kocatepe University Molecular Biology Department and Genetics laboratory. Bacterial suspensions prepared as 1.5×10^8 CFU/mL from 24 h cultures of microorganisms

Scheme 2 Synthesis of of poly(HEMA-co-FAOEME)

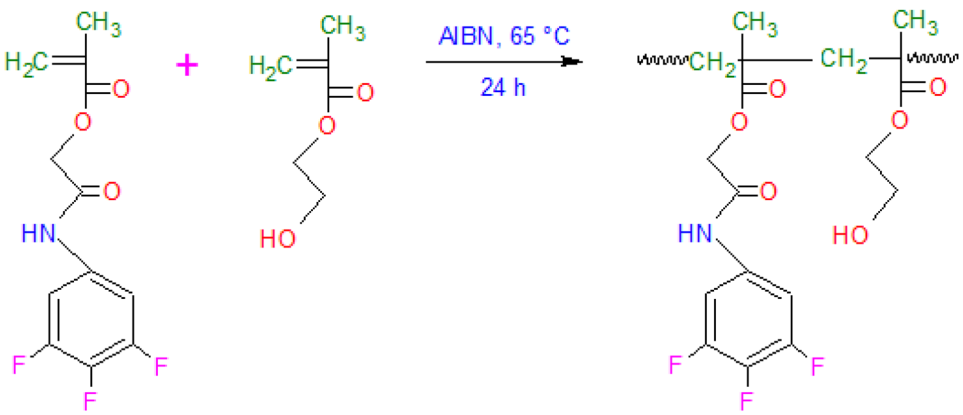

Table 1 Hydrothermal synthesis nanocomposites

Sample	poly(HEMA-co-FAOEME) (g)	ZnO (mg)	H_2O (mL)	T(°C)	Time (h)
3 w% ZnO	1	30			
5 w% ZnO	1	50	30	150	24
7 w% ZnO	1	70			

were spread homogeneously on Mueller Hinton Agar (MHA) (Merck, Almanya) using a steril swab. Ciprofloxacin against bacterial strains and Ketoconazole against yeasts were used as positive control, sterile distilled water was used as negative control and experiments were carried out in three parallels. Sterile empty antibiotic discs were placed on this agar and 10 µl of each dose were loaded onto it. Sterile blank antibiotic discs were placed on this agar and 10 µL of each dose were loaded on it and incubated at 37 °C for 72 h. The inhibition zones were measured at 24, 48 and 72 h.

Scratch wound assay

In this study, the effect of test substances on cell migration in wound healing in cell culture was investigated by the scratch wound test using human umbilical vein endothelial cells (HUVECs) [35]. The cells used in the study were cultured to a cell density of 35 mm (106 cells/mL) by adding 10% fetal bovine serum (HyClone, Logan, UT, USA) to RPMI 1640 (GIBCO, Uxbridge, UK) medium in each flask. 100 U/mL penicillin and 100 mg/mL streptomycin (Sigma, St. Louis, MO, USA) were added to the inactivated cell medium at 45 °C for 1 h and incubated at 37 °C in an incubator containing 5% CO_2 and the surface of the cells was 100% coating is allowed. In the wound healing experiment, a scratch-shaped cavity was created on a single cell layer that covered the entire floor %100. During this procedure, the medium was changed several times in order to remove the cells floating in the medium. At the end of the incubation period, it was determined whether the cells at the wound borders filled the wound.

Characterization techniques

The synthesis of nanocomposites was produced using the Fytronix 8000 fully automated nanomaterial fabrication system. X-ray diffraction *(*XRD*)* patterns of the prepared composites were recorded by a D8 Advance diffractometer Bruker (NanoSEM 650 model, detector: TLC) by using CuK_α radiation and a 2θ scan rate of 1.281°/min, in the 2θ range of 20°-80° by coating with gold film. NMR spectra of FAOEME and poly(HEMA-co-FAOEME) were recorded in DMSO-d6 solvent with a 400 MHz AVANCE III NMR spectrometer (Bruker Corp, Germany). Functional group analyzes of poly(HEMA-co-FAOEME) and nanocomposites were performed by FT-IR spectroscopy (Thermo Sci. Nicolet iS5, USA). TGA curves of the samples were obtained by using Shimadzu TG-60 (Japan) thermal analyzer in nitrogen atmosphere and approximately 7 mg samples in aluminum containers and heating up to 600 °C at a heating rate of 20 °C min^{-1} with the analyzer. The glass transition temperatures (Tg) of samples were determined using the DSC device (Shimadzu DSC-60, Japan) with a scanning speed of 10 °C min-1 in aluminum containers with approximately 8–10 mg of sample in a nitrogen environment up to 200 °C.

Results and discussion

Characterization of FAOEME

The FTIR spectrum of the FAOEME monomer is shown in Fig. 1. Characteristic amide and ester carbonyl carbonyl stretching vibrations of FAOEME were observed at 1677 cm^{-1} and 1724 cm^{-1}, respectively. The peaks observed at 2992 cm^{-1} are attributed to aliphatic C-H, and peaks observed at 3140 cm^{-1} are attributed to aromatic C-H stretching vibration bands. NH stretching vibration bands belonging to the amide group were observed at 3270 cm^{-1}.

The ^{1}H- and ^{13}C- NMR spectra of the FAOEME monomer are shown in Fig. 2 with the peak evaluations. Signals of vinyl protons characterizing the monomer appeared at 5.62 and 6.25 ppm. Signals of these protons were observed in the ^{13}C-NMR spectrum at 122 and 136 ppm,

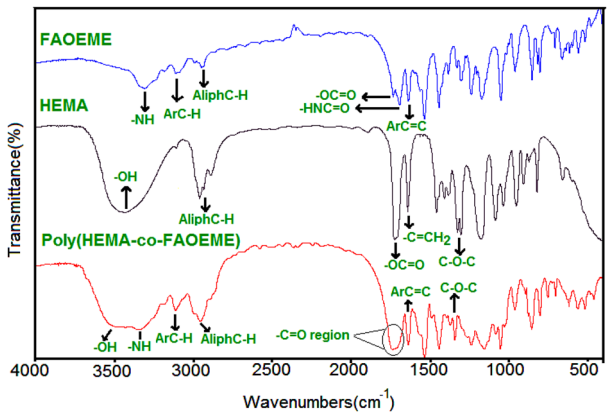

Fig. 1 The FTIR spectrum of the FAOEME monomer

respectively. In addition, the signals of ester and amide carbonyls appeared at 168 and 170 ppm, respectively. In conclusion, the ^{1}H- and ^{13}C- NMR spectra appear to agree with the structure of FAOEME.

Characterization of poly(HEMA-co-FAOEME)

The FTIR spectrum of poly(HEMA-co-FAOEME) is shown in Fig. 1. In the FT-IR spectrum, the ester carbonyl vibration band of HEMA at 1720 cm^{-1} and the bands of ester and amide carbonyl peaks at 1677 cm^{-1} and 1724 cm^{-1} in FAOEME units turned into a broad peak at 1730 cm^{-1} with copolymerization. In addition, the tension vibration bands observed in the range of 3200–3500 cm^{-1} belonging to the NH_2 and OH groups, both of which are found in two monomeric structures, became flattened around 3500 cm^{-1} with the copolymerization. The ^{1}H- and ^{13}C-NMR spectrum and evaluation of Poly(HEMA-co-FAOEME) are presented in Fig. 3. The characteristic peaks in the ^{1}H-NMR spectrum are the NH protons peaks at 10.15 pm and the OH groups

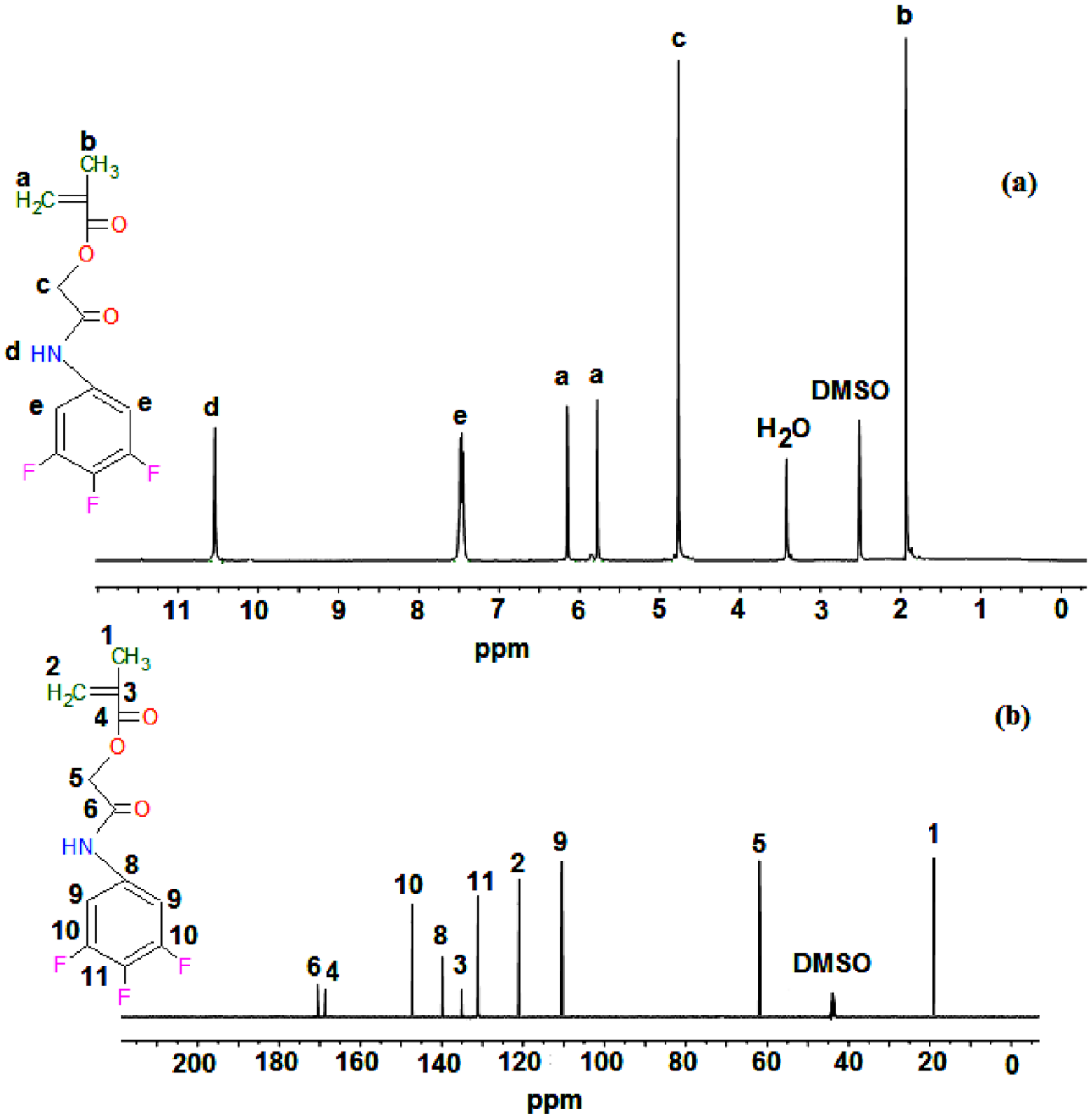

Fig. 2 The ^{1}H **a** and ^{13}C **b** - NMR spectra of the FAOEME

signals at 3.92 ppm. In addition, the absence of any signal between the vinyl proton region of 5.50 and 6.50 ppm indicates that the copolymer was successfully synthesized. In the ^{13}C-NMR spectrum of the copolymer, the amide and ester carbonyl peaks gave signals between 158 and 165 ppm. Aromatic carbons in FAOEME units were seen at 120–145 ppm. As can be seen from the ^{1}H- and ^{13}C-NMR spectrum data, the spectra are compatible with the copolymer structure.

Determination of poly(HEMA-co-FAOEME) composition

The copolymer composition was determined from the ratio of the integral height of the -NH units characteristic for FAOEME and signaling at 10.15 ppm to the integral height of the -OH units signaling at 3.92 ppm in HEMA units. From the calculations made, it was determined that there was 39% mole of FAOEME in the copolymer composition. The same

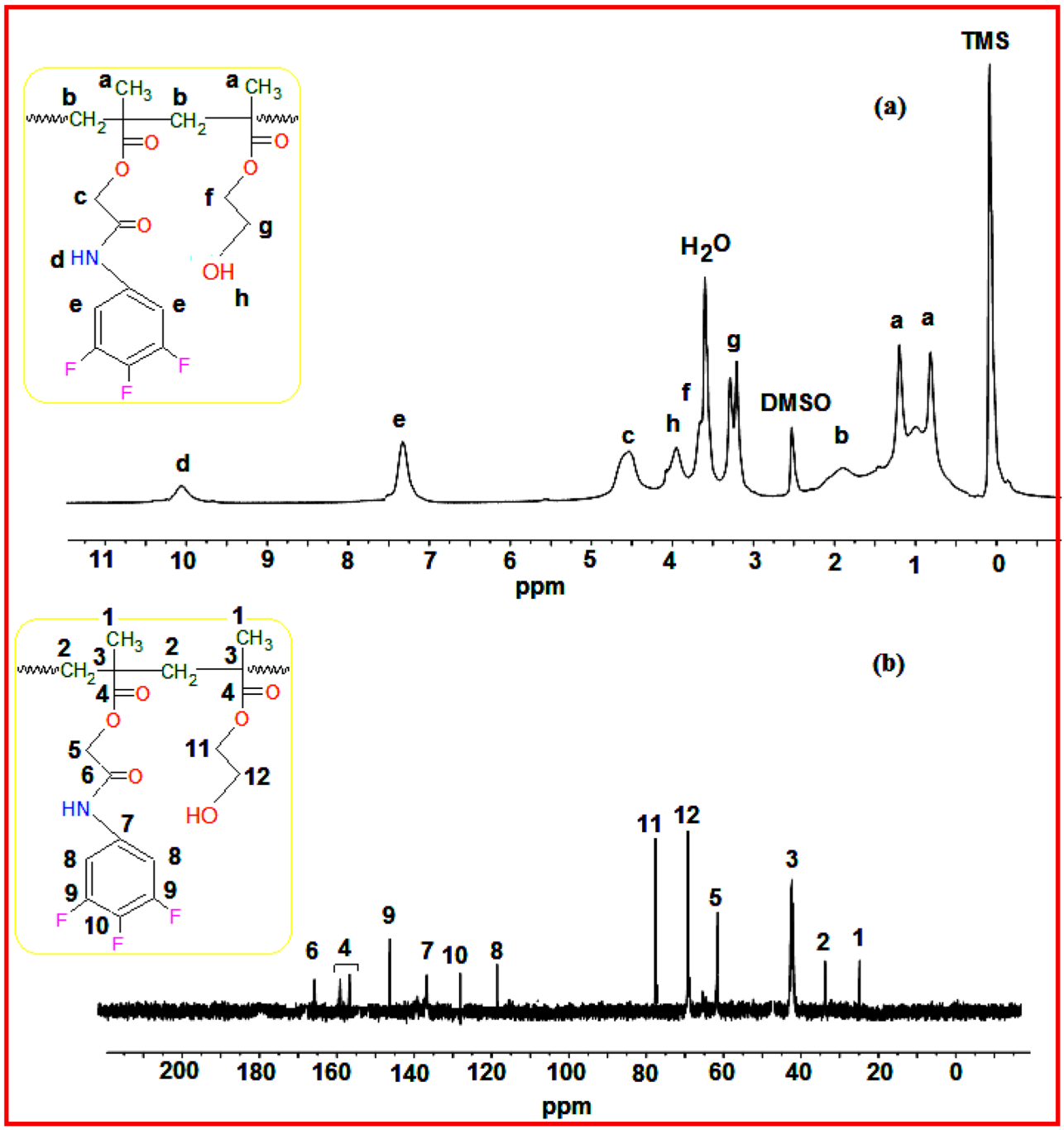

Fig. 3 The ^{1}H **a** and ^{13}C **b** -NMR spectrum and evaluation of Poly(HEMA-co-FAOEME)

result was confirmed in the determination of the nitrogen ratio in the copolymer composition by elemental analysis.

Characterization of the nanocomposites

XRD analyses

The X-ray diffraction patterns of poly(HEMA-co-FAOEME) and nanocomposites in the 20-80° range compared to ZnO nanoparticles are shown in Fig. 4. Since poly(HEMA-co-FAOEME) is an amorphous structure, it does not have any diffraction pattern. When the XRD patterns of nanocomposites are examined, it is seen that they mainly have Bragg peaks corresponding to (100), (002), (101), (102), (110), and 103 planes, and the diffraction patterns are 2θ = 31.85°, 34.75°, 36.72°, 46.75° 57.73° and 63.12°. The characteristic set of diffraction peaks detected in the XRD pattern confirms the hexagonal wurtzite structure of ZnO. It can be said that the diffraction peaks of ZnO are compatible with the 36-1451 numbered JCPDS data [36]. The mean crystal size of ZnO nanoparticles was found to be 34.17 nm by the Scherrer equation [37]. From the XRD patterns of the nanocomposites, the presence of ZnO nanoparticles in the copolymer matrix was confirmed by the characteristic peaks of ZnO. As the ZnO concentration in the copolymer matrix increases, the increase in the intensity of the ZnO peaks supports the proportional distribution of the nanoparticles in the matrix.

SEM and EDX analysis

SEM images of ZnO nanoparticles, poly(HEMA-co-FAOEME) and nanocomposites are shown in Fig. 5. SEM image of poly(HEMA-co-FAOEME) presents a characteristic surface

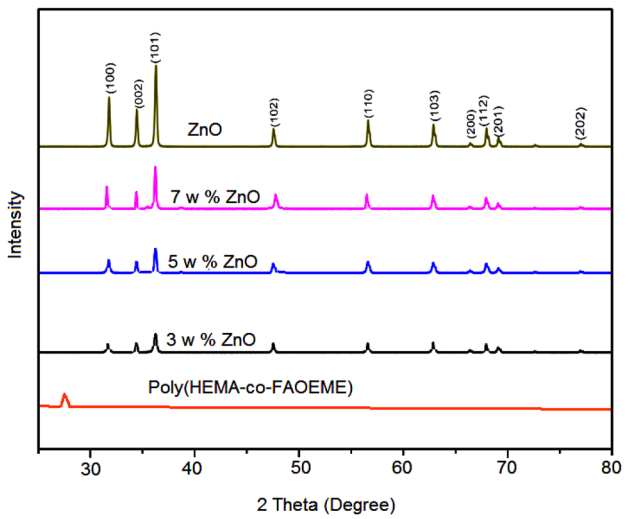

Fig. 4 The X-ray diffraction patterns of poly(HEMA-co-FAOEME) and nanocomposites

image for random copolymer. While the copolymer surface generally consists of rough areas, there are slight pits in some areas. The main reason for the difference in the morphology of these polymers can be attributed to the changes in the growth pattern of the polymer chain and the degree of polymerization. SEM images of biosynthesized ZnO nanoparticles appear to retain a number of major active molecules originating from *Mentha pulegium* L. These regions are shown in red circles in the SEM image. In the SEM images of the nanocomposites, it is seen that ZnO nanoparticles are mostly located on the copolymer matrix surface and are homogeneously dispersed without any aggregation. The dispersion in the nanocomposite containing 5% ZnO is remarkably better than the others. It can be said that a good distribution is achieved due to the strong hydrogen bonds between functional groups such as ketone contained in the main active groups carried by the ZnO nanoparticles from the *Mentha pulegium* L. (pulegone and mentone), and the -F, -OH, -HN, and ester groups contained in poly(HEMA-co-FAOEME). In addition, the probability of formation of strong H bonds between the hydroxyl groups on the ZnO surface and the fluorine atoms is quite high. Also, the effect of high temperature and pressure in the hydrothermal method caused ZnO nanoparticles to show a more regular distribution on the matrix surface. Similar results have been seen in some recent studies [38–40].

SEM-EDX analyzes of poly(HEMA-co-FAOEME) and nanocomposites are presented in Fig. 6. The EDX analysis of Poly(HEMA-co-FAOEME) shows the presence of carbon, oxygen, nitrogen and fluorine atoms in the selected region. EDX analysis of the nanocomposites confirms the presence and proportional distribution of the ZnO in the composite. While the wt% content of the Zn in the selected region in the nanocomposite containing 3% ZnO was 3.28, the same value increased to 82.85 in the nanocomposite containing 7% ZnO.

FT-IR analyses

The FTIR spectra of the poly(HEMA-co-FAOEME), ZnO, and nanocomposites are shown in Fig. 7 with their evaluation. The wide peak observed around 3500 cm^{-1} in the FTIR spectrum of ZnO nanoparticles belongs to the O-H stretching vibrations formed on the ZnO surface during the synthesis phase. The absorption band representing the spherical Zn-O stretching vibration was observed at 520 cm^{-1} [41]. The peak observed at 1720 cm^{-1} is probably attributed to the stretch vibration bands of ketone groups in pulegone and Mentone molecules, which are active components of *Mentha pulegium* L. Aromatic C = C vibrations bands peaked at 1630 cm^{-1}.

With the addition of the ZnO nanoparticles to the copolymer matrix, changes in the intensity of some peaks were observed. The presence of the ZnO in the nanocomposite was confirmed by the presence of the peak at 520 cm^{-1}, and the peaks in the carbonyl region of 1650–1730 cm^{-1} were broadened. This is due to the overlap of the amide and

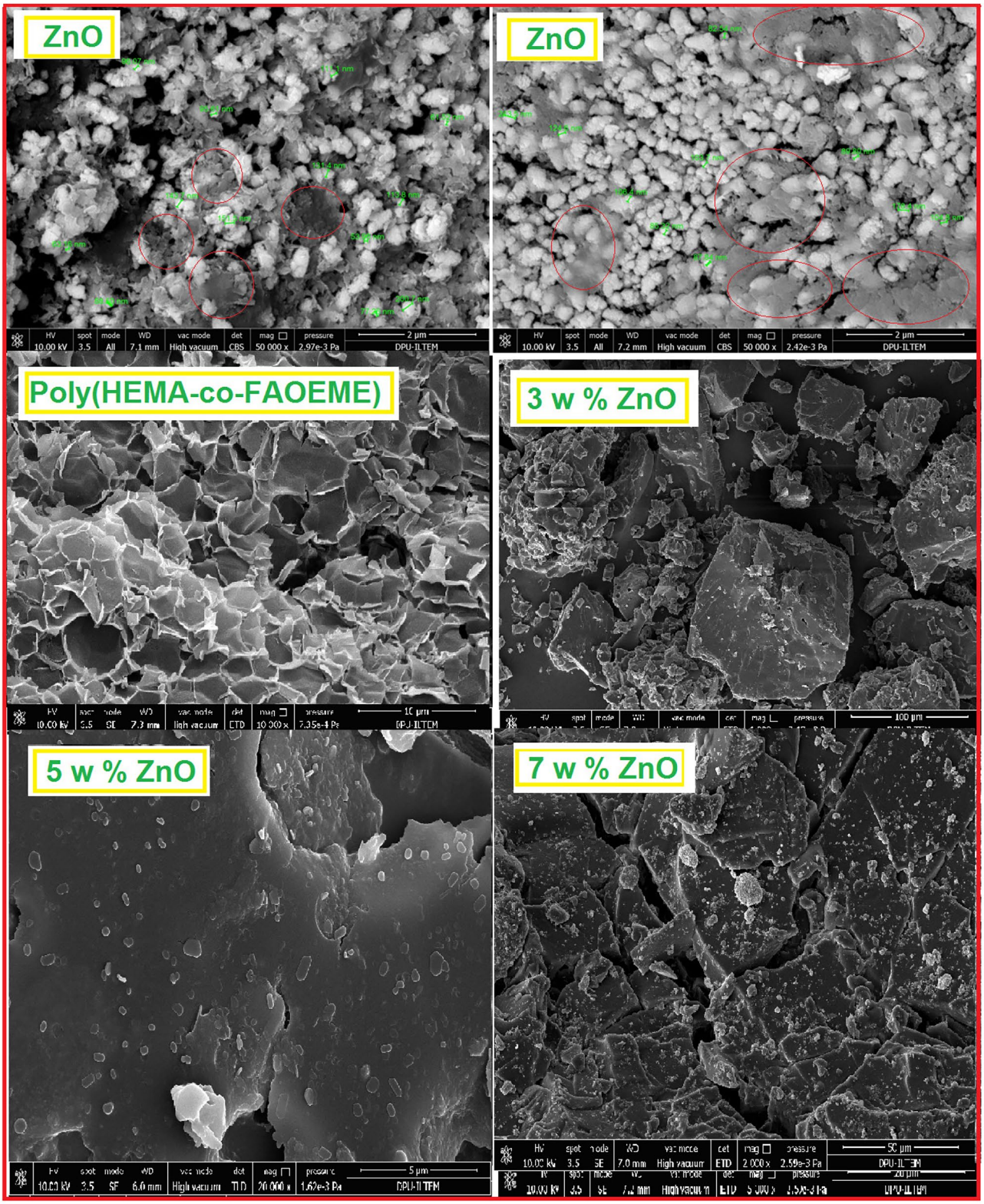

Fig. 5 SEM images of ZnO nanoparticles, poly(HEMA-co-FAOEME) and nanocomposites

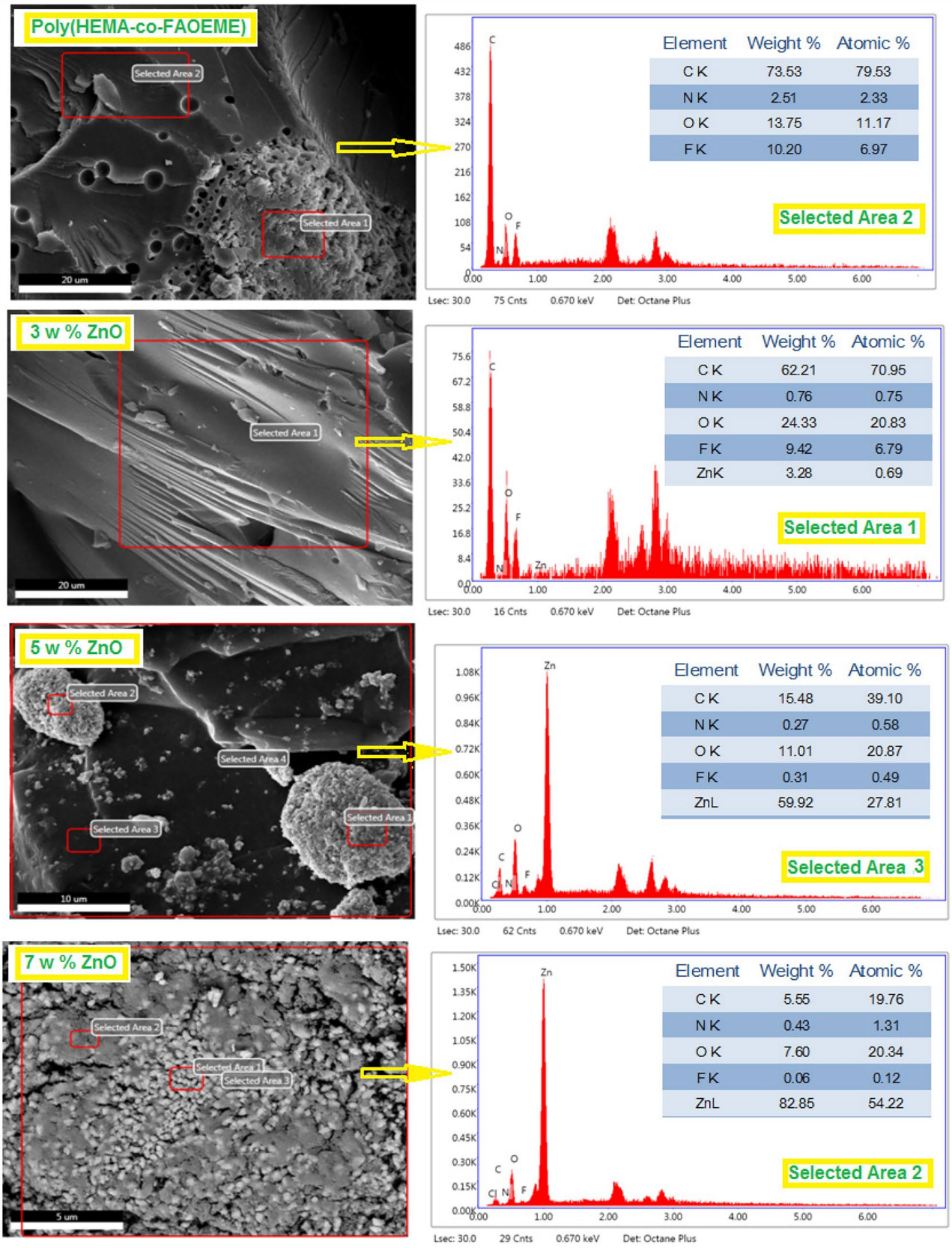

Fig. 6 SEM-EDX analyzes of poly(HEMA-co-FAOEME) and nanocomposites

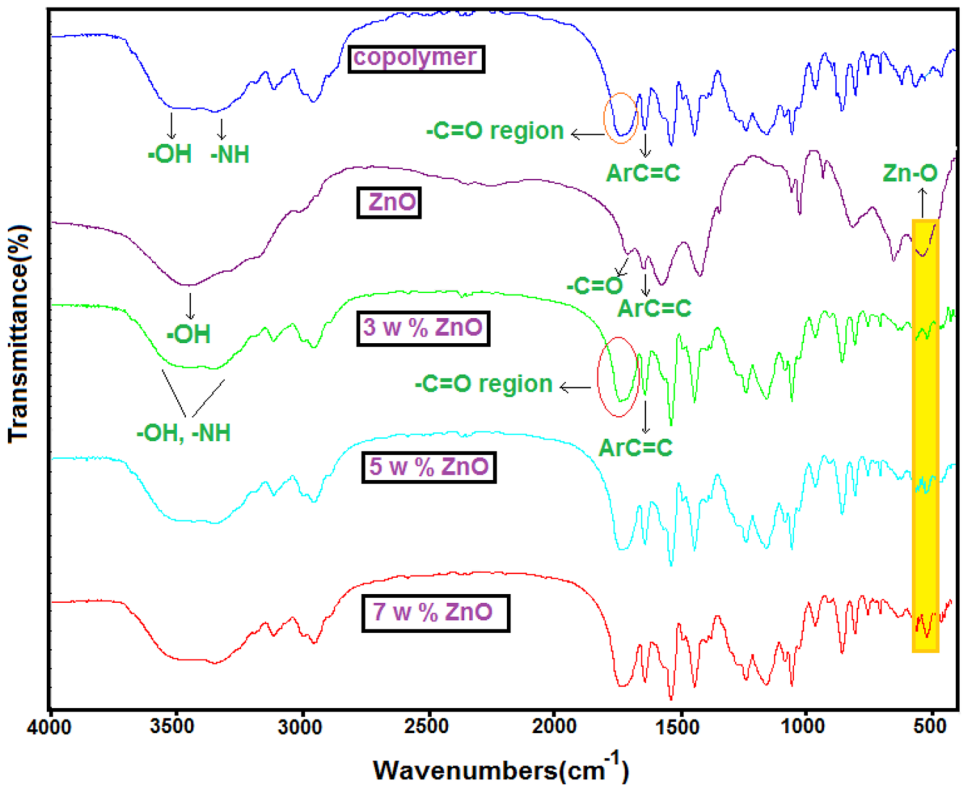

Fig. 7 The FTIR spectra of the copolymer, ZnO, and nanocomposites

ester carbonyls in the copolymer structure and the ketone groups held by the ZnO in the same region. The same situation was observed around 3600 cm^{-1}, the region of the tension vibration bands of -NH and -OH groups. As the ZnO concentration in poly(HEMA-co-FAOEME) increased, an increase was observed in the Zn-O stretching vibration band at 520 cm^{-1}. The results from FTIR show that ZnO nanoparticles are successfully dispersed in the copolymer matrix.

DSC analyses

Figure 8 shows the change in glass transition temperature (Tg) of poly(HEMA-co-FAOEME) and nanocomposites. Tg values were obtained from the DSC thermograms. The Tg value of the poly(HEMA-co-FAOEME) was measured as 127 °C. The Tg value of the poly(HEMA-co-FAOEME) was increased by the addition of ZnO nanoparticles. The Tg value, which was 98 °C with the addition of 3 w % ZnO nanoparticles, increased to 112 °C with an increase of 17 °C with the addition of 7 w % ZnO. In the literature, it has been reported that metal oxides added to polymers generally cause an increase in the Tg value of the pure polymer [42].

One of the reasons for this situation is the immobilization of ZnO nanoparticles on the surface of the Poly(HEMA-co-FAOEME). Immobilized ZnO nanoparticles limit the chain mobility of the copolymer matrix, causing a decrease in free volume and an increase in Tg value [43]. In the literature, it has been reported that fillers such as ZnO act as cross-linking agents, inhibiting the movement of polymer chains, thus causing an increase in the energy required to reach the glass transition region and an increase in Tg value [44].

In addition, another reason for the increase in Tg values of nanocomposites is the strong hydrogen bonds formed between Poly(HEMA-co-FAOEME) and ZnO nanoparticles. In particular, strong hydrogen bonds can form between the three fluorine atoms in the side branch of Poly(HEMA-co-FAOEME) and the hydroxyl groups on the surface of ZnO.

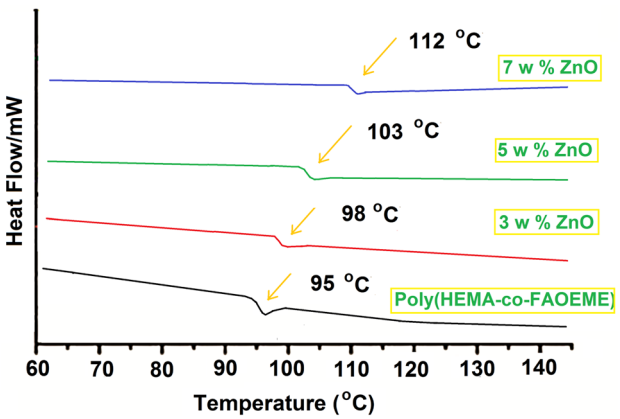

Fig. 8 DSC curve of poly(HEMA-co-FAOEME) and nanocomposites

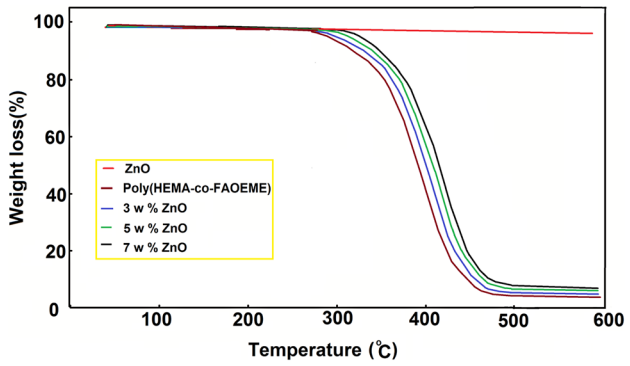

Fig. 9 TGA plot of poly(HEMA-co-FAOEME), ZnO, and nanocomposites

There are many studies showing that the Tg values of nanocomposites increase due to the H bond [38–40, 45].

TGA analyses

The thermal behaviors of poly(HEMA-co-FAOEME), ZnO, and nanocomposites were determined by heating them to 600 °C in a nitrogen atmosphere with TGA. The obtained thermograms are shown in Fig. 9. In addition, some thermal data of the samples are presented in Table 2. It was observed that poly(HEMA-co-FAOEME) decomposed in one step from the TGA curve, and the initial thermal decomposition temperature was 285 °C. In addition, the % residue left at 600 °C was 2.1. Heat treatment of polymers can affect either the bonds of the main chain (usual carbon to carbon bonds) or the side chains. Cleavage of the main chain usually yields free radicals, and either random or weak bond breaks are observed in the chain. Chain ends are also generally unstable structures suitable for initiating thermal degradation.

In the literature, the degradation mechanism of polymers with similar structures has been studied in detail. It has been determined that the thermal decomposition of poly(methacrylate esters) containing amide in the side branch begins with depolymerization and then continues with the formation of cyclic anhydride structures [46].

Table 2 TGA results of poly(HEMA-co-FAOEME) and nanocomposities

Sample	$^{a}T_i$/°C	$^{b}T_f$/°C	$^{c}T_{\%50}$/°C	Residue (%)
Poli(HEMA-co-FAOEME)	285	487	380	2.1
3 w % ZnO	291	491	405	4.9
5 w % ZnO	299	495	422	7.1
7 w % ZnO	304	500	433	9.2

a: Initial decomposition temperature

b: Temperature of final decomposition

c: Temperatures at %50 weight losses

It was observed that the thermal stability of Poly(HEMA-co-FAOEME) increased as the weight ratio of ZnO nanoparticles in the composite increased. While the initial decomposition temperature of the nanocomposite containing 3% by weight of ZnO was 291 °C, this value increased to 304 °C for the nanocomposite containing 7% by weight of ZnO.

The temperature value at which 50% mass loss occurs and the amount of residue also varies according to the amount of ZnO in the nanocomposite. While the temperature at which 50% mass loss occurs for pure poly(HEMA-co-FAOEME) was 380 °C, the same value increased to 433 °C with an increase of approximately 50 °C for nanocomposite containing 7% by weight ZnO filler.

Changes are observed in the physical and chemical properties of polymer nanocomposites obtained by adding nanoparticles to the polymer matrix, such as fire resistance and gas barrier properties [47]. In the literature has reported that metal oxide-based fillers act as a superior insulator and a sound mass transport barrier against volatile products formed during the thermal decomposition of matrices and act as a delayed "crosslinking agent" for the movement of matrix chains [48]. However, opposite results have been obtained in the literature. In the prepared Polystyrene/ZnO nanocomposites, it was observed that ZnO nanoparticles decreased the thermal decomposition initial temperature of the matrix. The reason for this result was attributed to the fact that ZnO NPs penetrated between the polymer chains and disrupted the chain interactions [49]. Another factor that increases the thermal stability can be strong hydrogen bonds between the three electronegative fluorine atoms in the structure of Poly(HEMA-co-FAOEME) and the -OH groups on the surface of ZnO nanoparticles [49].

Thermal degradation kinetics

The thermal decomposition activation energies of poly(HEMA-co-FAOEME) and nanocomposites were calculated using a TGA device with the Flynn-Fall-Ozowa method [50], which is one of the non-isothermal methods. For this purpose, TG curves of the samples were obtained at different heating rates (5, 10, 15 and 20 °C min^{-1}) in nitrogen atmosphere and the data obtained from these were used.

The TGA plot of poly(HEMA-co-FAOEME) at different heating rates is shown in Fig. 10. The E_a values were found according to the equation of FWO as given below:

$$\ln(\beta) = \ln\left(-\frac{AR}{R\ln(1-\alpha)}\right) - 5.331 - 1.052\frac{E_a}{R\,T} \quad (1)$$

In Eq. (1), R represents the gas constant, β represents the heating rate (°C min^{-1}), α the degree of transformation, and Ea the activation energy. According to the FWO method, Ea values are determined from the slope of the relationship

between log β and 1/T. The obtained FWO graph for Poly(HEMA-co-FAOEME) is as in Fig. 10.

The calculated Ea values of poly(HEMA-co-FAOEME) and nanocomposites at different conversion(α) are also presented in Table 3. The determined average Ea of poly(HEMA-co-FAOEME) is 132 kJ/mol. The calculated Ea values of the nanocomposites were higher than the value of Poly(HEMA-co-FAOEME) and increased with the ZnO concentration in the nanocomposite. As seen in Table 3, it was observed that the determined Ea values of the nanocomposites increased in parallel with the ZnO content they contained according to poly(HEMA-co-FAOEME). This result is probably due to the strong H bonds between the OH groups on the ZnO surface and the three F atoms in the Poly(HEMA-co-FAOEME) side branch.

Biological properties

The antimicrobial activity results of all the materials used in the study against some bacterial strains and *C. albicans* as a function of time are shown in Table 4. According to the antimicrobial activity results, it was observed that ZnO nanoparticles had a high antimicrobial effect in all microorganisms, except for *P. aeruginosa*, compared to other substances. In addition, it is observed that the antimicrobial effect increases more over time. For example, the diameter of the zone formed against *S. aureus* in 24 h increased from 15 to 19 mm at the end of 72 h. The same result is seen in other pathogens. The images of the zones formed by the materials are shown in Fig. 11.

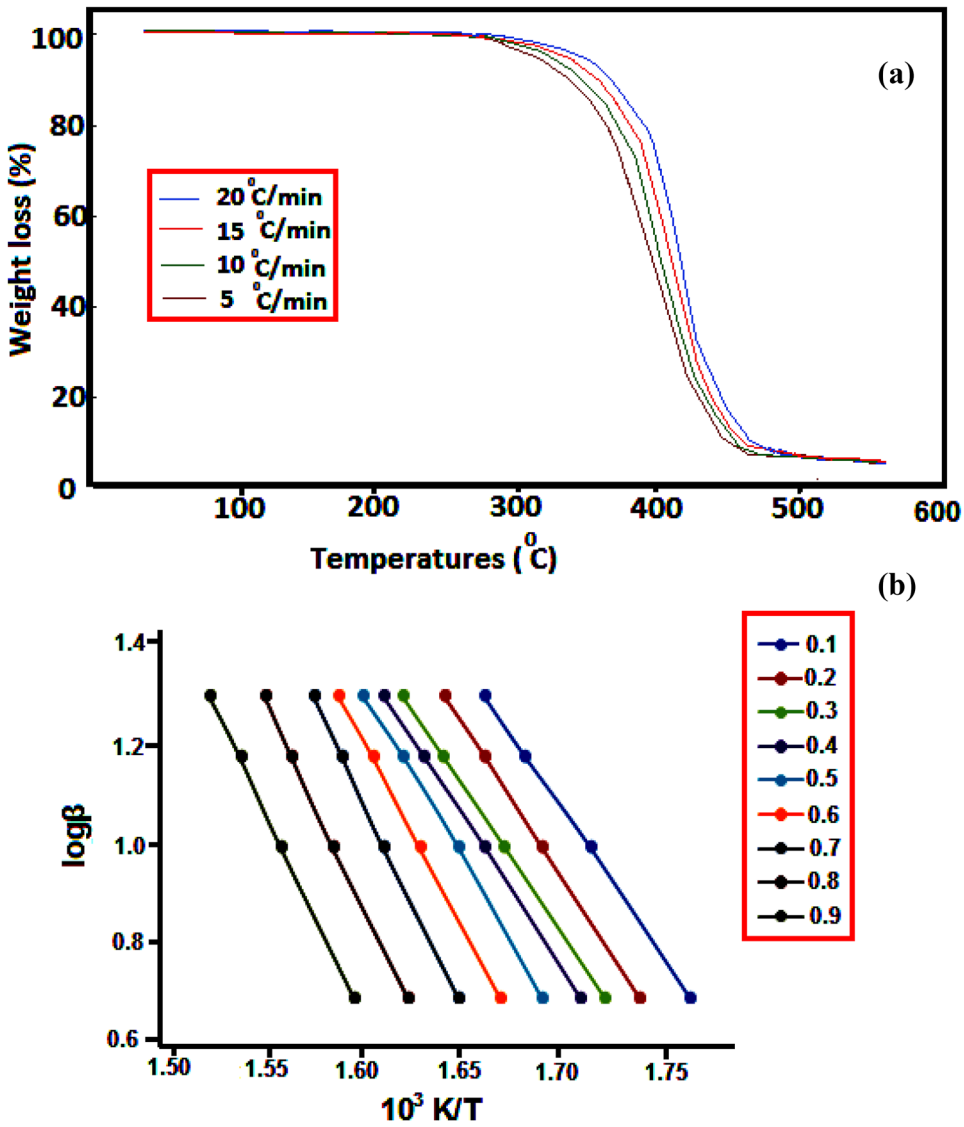

Fig. 10 The TGA thermograms of poly(HEMA-co-FAOEME) at different heating rates (**a**) and FWO plot (**b**)

Table 3 Ea values of poly(HEMA-co-FAOEME) and nanocomposites obtained by FWO method

Activation Energy (kJ/mol) at the Conversion (α)										
Sample	**0.1**	**0.2**	**0.3**	**0.4**	**0.5**	**0.6**	**0.7**	**0.8**	**0.9**	**Average**
poly(HEMA-co-FAOEME)	111	115	121	126	130	136	143	149	154	132
3 w % ZnO	115	121	129	136	140	144	150	155	160	139
5 w % ZnO	121	127	133	139	143	151	155	160	166	144
7 w % ZnO	127	132	136	143	150	155	161	164	172	149

Recent studies reveal that green synthesis ZnO NPs are a very useful and effective agent for the control of bacterial pathogens. It is also shown that this is a more specific and cost-effective method [51]. Today, antibiotics are the "gold standard" for the treatment of many bacterial infections [52, 53]. However, with the unconscious use of antibiotics, bacterial strains are highly likely to develop resistance to known antibiotics. This situation, which can pose a great problem in the treatment of diseases today, can only be eliminated by the synthesis of new antimicrobial substances [54]. For this reason, determination of the biological activities of nanomaterials is very important as it will also form the basis for drug design.

Another reason that increases the antimicrobial activity of ZnO NPs may be its biosynthesis from *Mentha pulegium L.* In recent years, a large number of investigations have been performed on antimicrobial activities of *Mentha* species [55–57]. Rad et al. [58] investigated the antimicrobial activity of nanoparticles obtained from *Mentha pulegium L.* by green synthesis in two strains (*E.coli and S. aureus*) and reported that they showed a significant antimicrobial effect on these microorganisms. In our study, 6 different strains were used. In parallel with the work of *E.coli* and *S. aereus*, antimicrobial activity was also detected. In addition, ZnO NP has antimicrobial activity in *E. faecalis, K. pneumoniae* and *C. albicans* microorganisms. Compared to this study, antimicrobial efficacy was found in our study, preferring a lower dose range of ZnO NP.

Antimicrobial activities of ZnO NPs against microorganisms vary depending on particle size, concentration, morphology, specific surface area, and characteristics of the microorganism. With the reduction of the fillers to nano size, the surface area of the filler increases and the specific properties of the filler are exhibited more efficiently in the composite material. This facilitates the interaction of bacteria and nanocomposites. The presence of a zone of

Table 4 The Antimicrobial Activities of ZnO, poly(HEMA-co-FAOEME) and nanocomposites

Strains	*Time (h)*	*3 w % ZnO*	*5 w % ZnO*	*7 w % ZnO*	*ZnO*	*Poli(HEMA-co-FAOEME*	*(-) Control*	*(+) Control*
E. coli	24	6	7	9	10	6	-	32
	48	7	8	9	11	7	-	33
	72	7	9	11	12	6	-	33
S. aureus	24	7	8	10	15	6	-	33
	48	8	9	10	19	7	-	34
	72	7	9	11	19	6	-	34
P. aeruginosa	24	-	-	-	6	-	-	40
	48	-	-	-	6	-	-	42
	72	-	-	-	6	-	-	45
E. faecalis	24	-	7	8	14	6	-	34
	48	-	7	9	15	6	-	36
	72	-	8	9	15	7	-	36
K. pneumoniae	24	6	7	8	13	6	-	44
	48	6	7	8	13	6	-	45
	72	6	8	9	13	6	-	45
C. albicans	24	6	7	8	9	6	-	37
	48	7	9	10	10	6	-	37
	72	7	8	9	11	6	-	37

(-) Control: distilled water, (+) control: strain-appropriate antibiotic

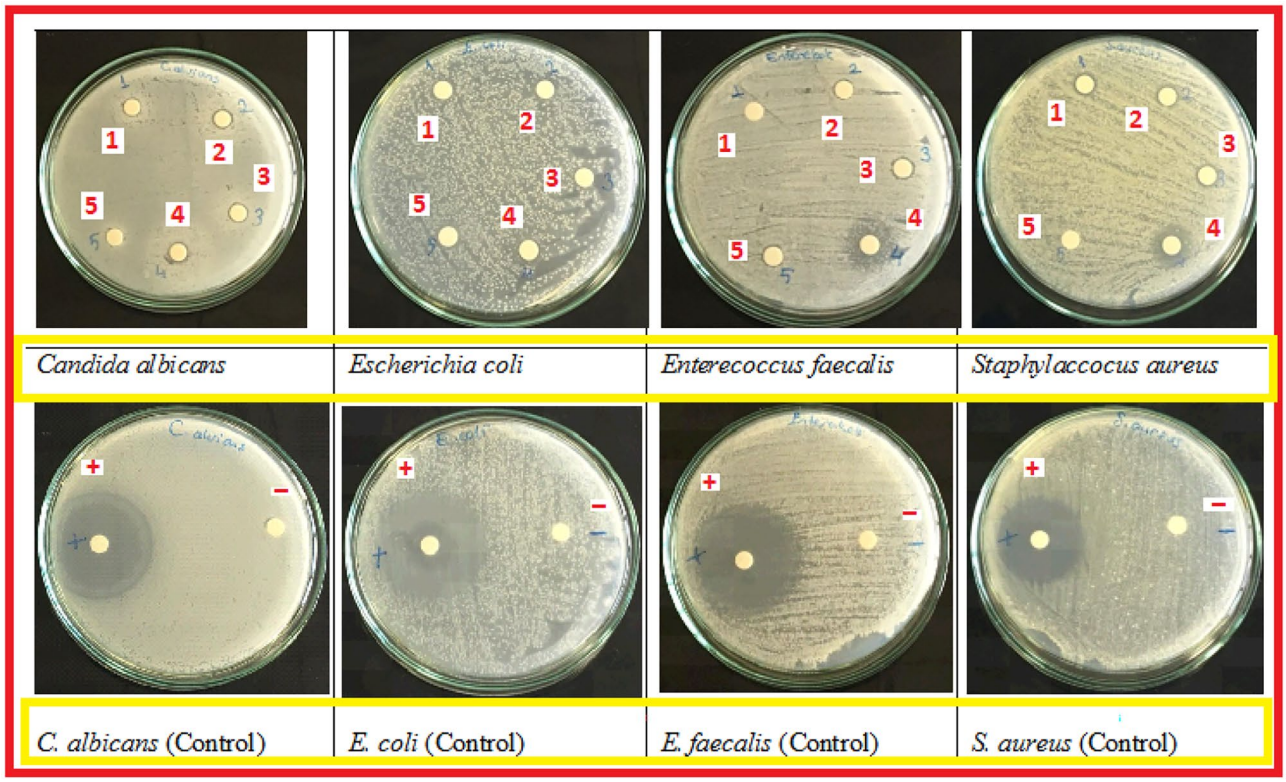

Fig. 11 The images of the zones formed by the materials

inhibition indicates that these particles drive pathogens to death through a mechanism that includes disruption of the microorganism's cell membrane. In order to overcome the problem of antimicrobial drug resistance, there is a need for new synthesized and reliable antibiotic substances. Evaluation of the biological activities of new synthesized nanoparticles to be obtained from different plants will form the basis of many studies in overcoming this problem.

The diameters of the zone formed by poly(HEMA-co-FAOEME), which is used as a matrix against pathogens, are generally between the diameters of ZnO NPs and nanocomposites. This shows that the antimicrobial effects of nanocomposites depend on the ZnO NPs concentration they contain. In general, it was observed that all nanocomposites did not show any effect against *P. aeruginosa* pathogen, as in ZnO NPs. Antimicrobial activity against other bacteria and *C. albicans* increases with time and with the proportion of ZnO NPs in the nanocomposite. From the results obtained, it can be said that the antimicrobial effects of nanocomposites depend on biosynthesized ZnO NPs.

There are findings in the literature that are in line with our results. It has been determined that composites containing ZnO NPs of polymers such as polyethylene [59], chitosan [60], polylactic acid [61], and polypropylene [62], which are especially used as food packaging materials, can prevent the growth of microorganisms that cause deterioration and prolong their shelf life. It has also been found that different ZnO polymeric nanocomposites have promising effects for wound healing and marine antifouling applications [63].

Wound healing properties of the materials

In this study, the curative properties of the test substances used in the experiment on HUVECs were investigated. Wound healing for Huvecs has been observed with the live cell imaging system and it has been determined that the cell lines contribute to wound closure by showing migration movements over time in this system. As seen in Fig. 12, although the effect of nanocomposites on cell migration is better than pure nanoparticles, it can be said that it is lower than the control group.

The most important process in skin healing is the transition of skin epithelial cells to epithelial-mesenchymal tissue. The skin consists of epithelial and mesenchymal cells. Skin epithelial cells pass into the mesenchymal tissue and differentiate into mesenchymal cells such as fibroblasts, smooth muscle cells of blood vessels, and pericytes. In this differentiation, a mesenchymal phenotype develops with molecular changes in skin epithelial cells. This change gives these cells the capacity to migrate to mesenchymal tissue, resist apoptosis, and produce a mesenchymal intercellular matrix.

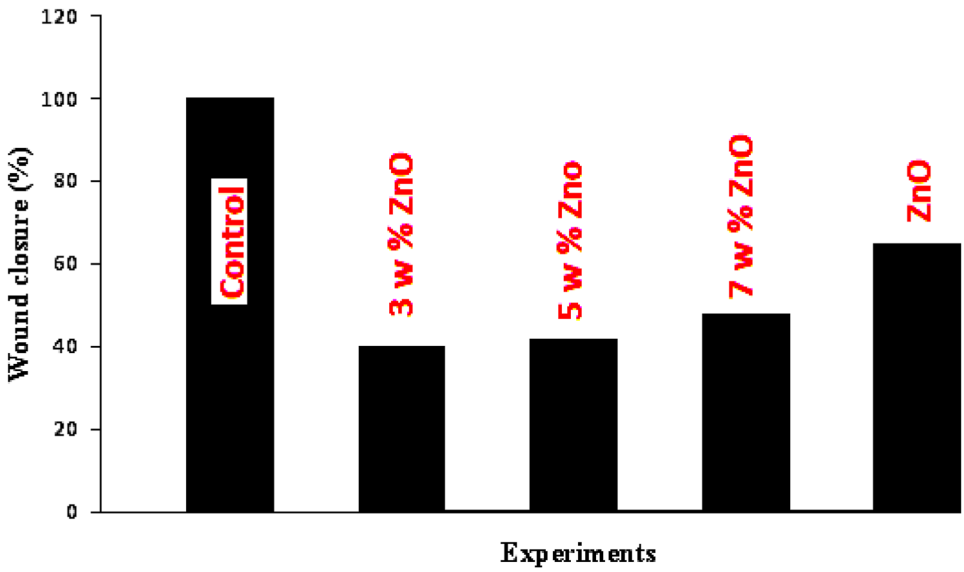

Fig. 12 Strach wound assay of ZnO and nanocomposites

Covering the skin, i.e. epithelialization is important in wound healing. This is associated with the proliferation and migration of epithelial cells adjacent to the wound towards the wound center. The epidermis at the wound edge thickens on the first day of injury. The marginal basal cells at the wound margin lose their attachment to the underlying dermis, enlarge and move to the surface of the temporary matrix. Cells at the wound edge proliferate rapidly and move over each other (toward the wound area) to close the wound defect. This period is completed in 48 h in mild wounds, but this period is extended in wounds with more significant shortcomings. It is known that this process is controlled by loss of contact inhibition and by cytokines released from fibronectin and monomolecular immune cells. Images of the scratch wound test are presented in Fig. 13. The in vitro scratch test is an easy, economical, and well-developed method often preferred to study in vitro cell migration [51]. The method is based on creating a new artificial gap, called a scratch, on a single cell line. Cells at the edge of the formed gap move towards the opening to close this gap, and this movement continues until new cell-cell connections are re-established [64].

ZnO NPs are among the chemicals used in wound treatment. The scratch assay, which examines the migration capacity and speed of cells by measuring the spread of the cell population to a given area to test wound healing activity in vitro, relies on the formation of scars (scratches) in monolayer cells. When the effect of ZnO NPs and nanocomposites on wound healing was evaluated with the scratch test, it

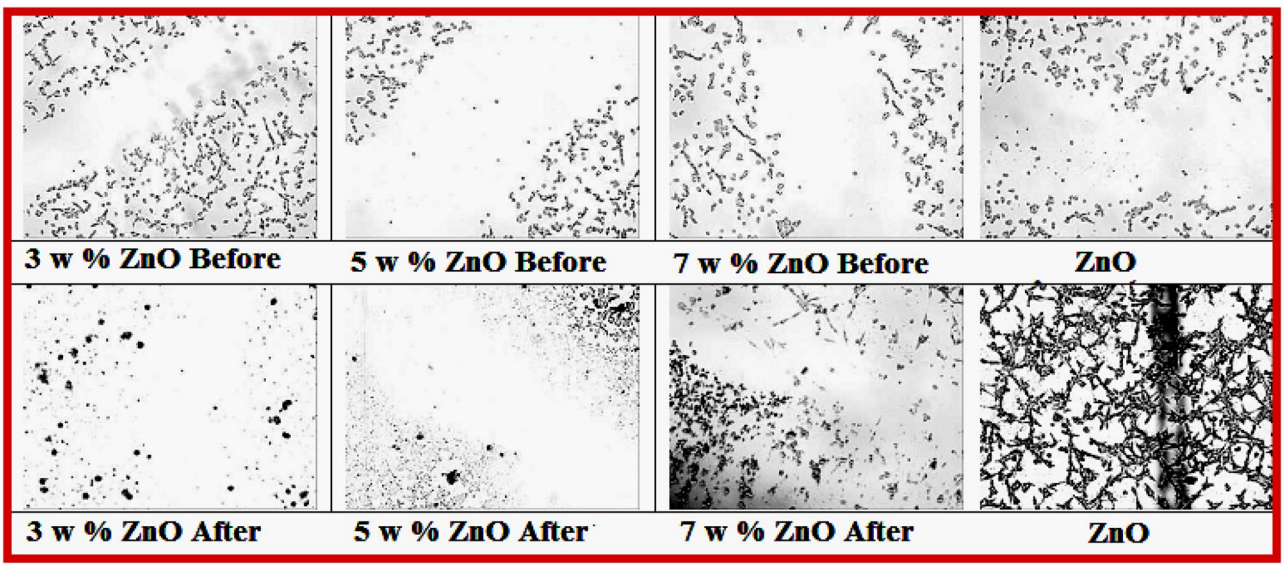

Fig. 13 Images of the scratch wound test of nanoparticles

was observed that the wound closure rate was slower in the group treated with the low-concentration mixture (3% and 5%). The wound closure rate was 7% and higher in ZnO NP groups. This situation reveals that ZnO NPs have an important effect on accelerating wound healing.

Conclusion

A copolymer of FAOEME monomer containing fluoroarylamide group in the side branch with HEMA was synthesized. Three nanocomposites of poly(HEMA-co-FAOEME) containing ZnO NP prepared by green synthesis were obtained by hydrothermal method. Structural characterization of FAOEME and Poly(HEMA-co-FAOEME) was performed by FTIR and NMR techniques. SEM, XRD, and FTIR analyzes of nanocomposites confirmed the presence and distribution of ZnO NPs in Poly(HEMA-co-FAOEME). TGA analyzes of nanocomposites clearly showed that the ZnO NPs improve the thermal stability of the Poly(HEMA-co-FAOEME). The thermal decomposition activation energies (Ea) of the nanocomposites were estimated by Flynn-Wall-Ozawa(FWO) method using non-isothermal TGA experiments. The glass transition temperature of poly(HEMA-co-FAOEME) increased from 95 ^{o}C to 112 ^{o}C thanks to ZnO NPs. It was observed that the antimicrobial effects of nanocomposites depend on the amount of ZnO NPs they contain. In addition, it was determined that nanocomposites have wound healing properties, and this property is due to ZnO NPs. The data showed that Poly(HEMA-co-FAOEME)/ZnO nanocomposites could be used as biomaterials.

Funding This study has been supported by the Afyon Kocatepe University Scientific Research Projects Coordination Unit. The Project Number is 22.FEN.BİL.33.

Declarations

Conflict of interest The authors declare that they have no known competing financial interests or personal relationships that could have appeared to influence the work reported in this paper.

References

1. Mouritz AP, Galos J, Linklater DP, Ladani RB, Kandare E, Crawford RJ, Ivanova EP (2021) Towards antiviral polymer composites to combat COVID-19 transmission. Nano Select 2(11):2061–2071. https://doi.org/10.1002/nano.202100078
2. Jeevanandam J, Krishnan S, Hii YS, Pan S, Chan YS, Acquah C, Rodrigues J (2022) Synthesis approach-dependent antiviral properties of silver nanoparticles and nanocomposites. J Nanostructure Chem 1–23. https://doi.org/10.1007/s40097-021-00465-y
3. Liu Q, Zhang Y, Liu W, Wang LH, Choi YW, Fulton M, Ma M (2021) A broad-spectrum antimicrobial and antiviral membrane inactivates SARS-CoV-2 in Minutes. Adv Funct Mater 31(47):2103477. https://doi.org/10.1002/adfm.202103477
4. Francolini I, Donelli G, Crisante F, Taresco V, Piozzi A (2015) Antimicrobial polymers for anti-biofilm medical devices: state-of-art and perspectives. Biofilm-based healthcare-associated infections. Springer, Cham, pp 93–117. https://doi.org/10.1007/978-3-319-09782-4
5. Behzadinasab S, Chin A, Hosseini M, Poon L, Ducker WA (2020) A surface coating that rapidly inactivates SARS-CoV-2. ACS Appl Mater Interfaces 12(31):34723–34727. https://doi.org/10.1021/acsami.0c11425
6. Youssef A vd (2016) Enhancement of Egyptian soft white cheese shelf life using a novel chitosan/carboxymethyl cellulose/zinc oxide bionanocomposite film. Carbohydrate Polym 15:9–19. https://doi.org/10.1016/j.carbpol.2016.05.023
7. Pérez-Altamar M, Perales-Pérez O (2014) Fabrication and characterization of chitosan/cellulose-ZnO nanocomposites for bactericidal applications. MRS Online Proc Library (OPL) 1685. https://doi.org/10.1557/opl.2014.690
8. Liu Q, Hedberg EL, Liu Z, Bahulekar R, Meszlenyi RK, Mikos AG (2000) Preparation of macroporous poly (2-hydroxyethyl methacrylate) hydrogels by enhanced phase separation. Biomaterials 21(21):2163–2169. https://doi.org/10.1016/S0142-9612(00)00137-X
9. Kumar A, Tyagi P, Singh H, Kumar Y, Lahiri SS (2012) Synthesis and characterization of a porous poly (hydroxyethylmethacrylate-co-ethylene glycol dimethacrylate)-based hydrogel device for the implantable delivery of insulin. J Appl Polym Sci 126(3):894–905. https://doi.org/10.1002/app.36531
10. Horák D, Hlídková H, Hradil J, Lapčíková M, Šlouf M (2008) Superporous poly (2-hydroxyethyl methacrylate) based scaffolds: Preparation and characterization. Polymer 49(8):2046–2054. https://doi.org/10.1016/j.polymer.2008.02.041
11. Zare M, Bigham A, Zare M, Luo H, Rezvani Ghomi E, Ramakrishna S (2021) pHEMA: an overview for Biomedical Applications. Int J Mol Sci 15(12):6376. https://doi.org/10.3390/ijms22126376
12. Torgut G, Yazdıç FC, Gürler N (2022) Synthesis, characterization, pH-sensitive swelling and antimicrobial activities of chitosan–graft-poly(hydroxyethyl methacrylate) hydrogel composites for biomedical applications. Polym Eng Sci 62:2552–2559. https://doi.org/10.1002/pen.26040
13. Sacher E (1994) Fluoropolymer metallization for microelectronic applications. Prog Surf Sci 47(3):273–300. https://doi.org/10.1016/0079-6816(94)90020-5
14. Pu FR, Williams RL, Markkula TK, Hunt JA (2002) Effects of plasma treated PET and PTFE on expression of adhesion molecules by human endothelial cells in vitro. Biomaterials 23(11):2411–2428. https://doi.org/10.1016/S0142-9612(01)00377-5
15. Erol I (2008) Novel methacrylate copolymers with fluorine containing: synthesis, characterization, reactivity ratios, thermal properties and biological activity. J Fluorine Chem 129(7):613–620. https://doi.org/10.1016/j.jfluchem.2008.05.002
16. Erol I, Sahin B (2015) Functional styrenic copolymer based on 2-(dimethylamino)ethyl methacrylate: reactivity ratios, biological activity thermal properties and semi-conducting properties. J Fluorine Chem 178:154–164. https://doi.org/10.1016/j.jfluchem.2015.07.002
17. Goh EG, Xu X, McCormick PG (2014) Effect of particle size on the UV absorbance of zinc oxide nanoparticles. Scripta Mater 78:49–52. https://doi.org/10.1016/j.scriptamat.2014.01.033
18. Da Silva BL, Caetano BL, Chiari-Andréo BG, Pietro RCLR, Chiavacci LA (2019) Increased antibacterial activity of ZnO nanoparticles: influence of size and surface modification. Colloids Surf B 177:440–447. https://doi.org/10.1016/j.colsurfb.2019.02.013
19. Evstropiev SK, Dukelskii KV, Karavaeva AV, Vasilyev VN, Kolobkova EV, Nikonorov NV, Evstropyev KS (2017) Transparent bactericidal ZnO nanocoatings. J Mater Science: Mater Med 28(7):102. https://doi.org/10.1007/s10856-017-5909-4

20. Singh P, Nanda A (2014) Enhanced sun protection of nano-sized metal oxide particles over conventional metal oxide particles: an in vitro comparative study. Int J Cosmet Sci 36(3):273–283. https://doi.org/10.1111/ics.12124
21. Nomoto JI, Hirano T, Miyata T, Minami T (2011) Preparation of Al-doped ZnO transparent electrodes suitable for thin-film solar cell applications by various types of magnetron sputtering depositions. Thin Solid Films 520(5):1400–1406. https://doi.org/10.1016/j.tsf.2011.10.003
22. Ghaffari H, Tavakoli A, Moradi A, Tabarraei A, Bokharaei-Salim F, Zahmatkeshan M, Ataei-Pirkooh A (2019) Inhibition of H1N1 influenza virus infection by zinc oxide nanoparticles: another emerging application of nanomedicine. J Biomed Sci 26:70:1–10. https://doi.org/10.1186/s12929-019-0563-4
23. Harley RM, Atkins S, Budantsev AL, Cantino PD, Conn BJ, Grayer R, Upson T (2004) Labiatae. Flowering Plants· Dicotyledons. Springer, Berlin, Heidelberg, pp 167–275. https://doi.org/10.1007/978-3-642-18617-2_11
24. Kamkar A, Javan AJ, Asadi F, Kamalinejad M (2010) The antioxidative effect of iranian Mentha pulegium extracts and essential oil in sunflower oil. Food Chem Toxicol 48(7):1796–1800. https://doi.org/10.1016/j.fct.2010.04.003
25. Jebali J, Ghazghazi H, Aouadhi C, ELBini-Dhouib I, Ben Salem R, Srairi-Abid N, Rigane G (2022) Tunisian native Mentha pulegium L. extracts: Phytochemical Composition and Biological Activities. Molecules 27(1):314. https://doi.org/10.3390/molecules27010314
26. Kogiannou DA, Kalogeropoulos N, Kefalas P, Polissiou MG, Kaliora AC (2013) Herbal infusions; their phenolic profile, antioxidant and anti-inflammatory effects in HT29 and PC3 cells. Food Chem Toxicol 61:152–159. https://doi.org/10.1016/j.fct.2013.05.027
27. Romero-Jiménez M, Campos-Sánchez J, Analla M, Muñoz-Serrano A, Alonso-Moraga Á (2005) Genotoxicity and anti-genotoxicity of some traditional medicinal herbs. Mutat Res/Genetic Toxicol Environ Mutagen 585(1–2):147–155. https://doi.org/10.1016/j.mrgentox.2005.05.004
28. Ibrahim AK (2013) New terpenoids from Mentha pulegium L. and their antimicrobial activity. Nat Prod Res 27(8):691–696. https://doi.org/10.1080/14786419.2012.691488
29. Mahboubi M, Haghi G (2008) Antimicrobial activity and chemical composition of Mentha pulegium L. essential oil. J Ethnopharmacol 119(2):325–327. https://doi.org/10.1016/j.jep.2008.07.023
30. Erol I, Gürler Z (2022) A new methacrylate polymer functionalized with fluoroarylketone prepared by hydrothermal method and its nanocomposites with SiO2: thermal, dielectric, and biocidal properties. Polym Bull 1–24. https://doi.org/10.1007/s00289-022-04195-1
31. Erol I, Hazman Ö, Aksu M, Bulut E (2022) Synergistic effect of ZnO nanoparticles and hesperidin on the antibacterial properties of chitosan. J Biomater Sci Polym Ed 1–25. https://doi.org/10.1080/09205063.2022.2099668
32. Montheard JP, Chatzopoulos M, Chappard D (1992) 2-hydroxyethyl methacrylate (HEMA): chemical properties and applications in biomedical fields. J Macromolecular Sci Part C: Polym Reviews 32(1):1–34. https://doi.org/10.1080/15321799208018377
33. Erol I, Özcakir R, Gürler Z (2015) Novel functional methacrylate copolymers with side chain tertiary amine and alkynes and their some properties. J Polym Res 22:635. https://doi.org/10.1007/s10965-014-0635-9
34. Bauer AW (1966) Antibiotic susceptibility testing by a standardized single disc method. Am J clin pathol 45(4):149–158
35. Heller RB, McGannon J, Weber AH (1950) Precision determination of the lattice constants of zinc oxide. J Appl Phys 21(12):1283–1284. https://doi.org/10.1063/1.1699591
36. Sinha A, Sharma BP (2002) Preparation of copper powder by glycerol process. Mater Res Bull 37(3):407–416. https://doi.org/10.1016/S0025-5408(01)00819-4
37. Erol I, Cigerci IH, Özkara A, Akyıl D, Aksu M (2022) Synthesis of moringa oleifera coated silver-containing nanocomposites of a new methacrylate polymer having pendant fluoroarylketone by hydrothermal technique and investigation of thermal, optical, dielectric and biological properties. J Biomater Sci Polym Ed 33:101231–101255. https://doi.org/10.1080/09205063.2022.2046986
38. Erol İ, Yurdakal S, Demirelli K, Gürler Z (2022) Preparation of PHEMA/TiO2 nanocomposites by combination of in-situ polymerization/hydrothermal method and determination of their thermal, swelling, biological and dielectric properties. J Polym Res 29(7):281. https://doi.org/10.1007/s10965-022-03146-8
39. Erol I, Aksu M, Gürler Z (2022) Preparation of poly (AAm-co-HEMA)/ZnO nanocomposites via in situ polymerization/hydrothermal method and determination of their properties. Polym Bulletin 1–29. https://doi.org/10.1007/s00289-022-04343-7
40. Demirelli K, Coşkun M, Erol I (2000) Copolymerization and monomer reactivity ratios of 2-(3-mesityl-3-methylcyclobutyl)-2-hydroxyethyl methacrylate with acrylonitrile. Eur Polymer J 36(1):83–88. https://doi.org/10.1016/s0014-3057(99)00039-7
41. Lee J, Bhattacharyya D, Easteal AJ, Metson JB (2008) Properties of nano-ZnO/poly (vinyl alcohol)/poly (ethylene oxide) composite thin films. Curr Appl Phys 8(1):42–47. https://doi.org/10.1016/j.cap.2007.04.010
42. Aldosari MA, Othman AA, Alsharaeh EH (2013) Synthesis and characterization of the in situ bulk polymerization of PMMA containing graphene sheets using microwave irradiation. Molecules 18(3):3152–3167. https://doi.org/10.3390/molecules18033152
43. Džunuzović E, Marinović Cincović M, Vuković J, Jeremić K, Nedeljković JM (2009) Thermal properties of PMMA/TiO_2 nanocomposites prepared by in situ bulk polymerization. Polym Compos 30(6):737–742. https://doi.org/10.1002/pc.20606
44. Wu CS (2007) Characterizing polycaprolactone/SiO_2–TiO_2 nanocomposites synthesized via in situ sol–gel polymerization. Des Monomers Polym 10(4):311–326. https://doi.org/10.1163/156855507781505129
45. Mishra RS, Mishra AK, Raju KVSN (2009) Synthesis and property study of UV-curable hyperbranched polyurethane acrylate/ZnO hybrid coatings. Eur Polymer J 45(3):960–966. https://doi.org/10.1016/j.eurpolymj.2008.11.023
46. Coşkun M, Erol İ, Coşkun MF, Demirelli K (2002) Thermal degradation behaviour of two methacrylate polymers with side chain amide groups. Polym Degrad Stab 78(1):49–55. https://doi.org/10.1016/s0141-3910(02)00118-0
47. Hradil J, Horák D (2005) Characterization of pore structure of PHEMA-based slabs. React Funct Polym 62(1):1–9. https://doi.org/10.1016/j.reactfunctpolym.2004.08.007
48. Erol I, Deveci T (2021) Novel methacrylate copolymers functionalized with fluoroarylamide; copolymerization kinetics, thermal stability and antimicrobial properties. J Biomater Sci Polym Ed 32(14):1810–1834. https://doi.org/10.1080/09205063.2021.1938858
49. Hong RY, Qian JZ, Cao JX (2006) Synthesis and characterization of PMMA grafted ZnO nanoparticles. Powder Technol 163(3):160–168. https://doi.org/10.1016/j.powtec.2006.01.015
50. Ozawa T (1965) A new method of analyzing thermogravimetric data. Bull Chem Soc Jpn 38(11):1881–1886. https://doi.org/10.1246/bcsj.38.1881
51. Rad SS, Sani AM, Mohseni S (2019) Biosynthesis, characterization and antimicrobial activities of zinc oxide nanoparticles from leaf extract of Mentha pulegium (L.). Microb Pathog 131:239–245. https://doi.org/10.1016/j.micpath.2019.04.022
52. Davies J, Davies D (2010) Origins and evolution of antibiotic resistance. Microbiol Mol Biol Rev 74(3):417–433. https://doi.org/10.1128/MMBR.00016-10
53. Cavalieri F, Tortora M, Stringaro A, Colone M, Baldassarri L (2014) Nanomedicines for antimicrobial interventions. J Hosp Infect 88(4):183–190. https://doi.org/10.1016/j.jhin.2014.09.009

54. Hussain AI, Anwar F, Nigam PS, Ashraf M, Gilani AH (2010) Seasonal variation in content, chemical composition and antimicrobial and cytotoxic activities of essential oils from four Mentha species. J Sci Food Agric 90(11):1827–1836. https://doi.org/10.1002/jsfa.4021
55. Erol I, Sanli G, Dİlek M, Ozcan L (2010) Synthesis and characterization of novel methacrylate copolymers based on sulfonamide and coumarine: Monomer reactivity ratios, biological activity, thermal stability, and optical properties. J Polym Sci Part A: Polym Chem 48(19):4323–4334. https://doi.org/10.1002/pola.24220
56. Moldovan RI, Oprean R, Benedec D, Hanganu D, Duma M, Oniga I, Vlase L (2014) LC-MS analysis, antioxidant and antimicrobial activities for five species of Mentha cultivated in Romania. Digest J Nanomaterials Biostructures 9(2):559–566
57. Barchan A, Bakkali M, Arakrak A, Laglaoui A (2016) Effet antibactérien et anti-biofilm de trois espèces de Mentha: Mentha spicata, Mentha pulegium et Mentha piperita. Phytothérapie 14(2):88–96. https://doi.org/10.1007/s10298-015-0970-y
58. Park YJ, Baskar TB, Yeo SK, Arasu MV, Al-Dhabi NA, Lim SS, Park SU (2016) Composition of volatile compounds and in vitro antimicrobial activity of nine Mentha spp. Springerplus 5(1):1–10. https://doi.org/10.1186/s40064-016-3283-1
59. Chang BP, Akil HM, Nasir RBM, Bandara IMCCD, Rajapakse S (2014) The effect of ZnO nanoparticles on the mechanical, tribological and antibacterial properties of ultra-high molecular weight polyethylene. J Reinf Plast Compos 33(7):674–686. https://doi.org/10.1177/0731684413509426
60. Al-Naamani L, Dobretsov S, Dutta J (2016) Chitosan-zinc oxide nanoparticle composite coating for active food packaging applications. Innov Food Sci Emerg Technol 38:231–237. https://doi.org/10.1016/j.ifset.2016.10.010
61. Mousa HM, Abdal-Hay A, Bartnikowski et al (2018) A multifunctional zinc oxide/poly(lactic acid) nanocomposite layer coated on magnesium alloys for controlled degradation and antibacterial function. ACS Biomater Sci Eng 4:62169–62180. https://doi.org/10.1021/acsbiomaterials.8b00277
62. Silvestre C, Cimmino S, Pezzuto M et al (2013) Preparation and characterization of isotactic polypropylene/zinc oxide microcomposites with antibacterial activity. Polym J 45(9):938–945. https://doi.org/10.1038/pj.2013.8
63. Cahú TB, Silva RA, Silva RPF et al (2017) Evaluation of chitosan-based films containing gelatin, chondroitin 4-sulfate and ZnO for wound healing. Appl Biochem Biotechnol 183(3):765–777. https://doi.org/10.1007/s12010-017-2462-z
64. Todaro GJ, Lazar GK, Green H (1965) The initiation of cell division in a contact-inhibited mammalian cell line. J Cell Comp Physiol 66(3):325–333. https://doi.org/10.1002/jcp.1030660310